5.3 SPATIAL CORRELATION OF SURFACE-LEVEL VARIABLES OVER ARCTIC SEA ICE

Edgar L Andreas*
NorthWest Research Associates, Inc.; Lebanon, New Hampshire

and

Rachel E. Jordan
Jordan Environmental Modeling, PC; Hanover, New Hampshire

1. INTRODUCTION

Global climate models and numerical weather prediction models are divided into horizontal grid cells that range in size from a few kilometers to 100 km (e.g., Collins et al. 2006; Hunke et al. 2010; Bromwich et al. 2009; Tastula et al. 2012). The working assumption in such models is that atmospheric variables have the same value over an entire grid cell. For example, the 2-meter air temperature is taken to be the same value over a climate model grid cell that may be 100 km on a side. We have data from the experiment to study the Surface Heat Budget of the Arctic Ocean (SHEBA; Uttal et al. 2002) to assess how appropriate this assumption of grid cell uniformity is over Arctic sea ice.

During the year-long SHEBA deployment (October 1997 to October 1998), the Atmospheric Surface Flux Group (ASFG; Andreas et al. 1999; Persson et al. 2002) maintained five sites with separations from one another of up to 12 km. By correlating simultaneous data between pairs of sites, we can evaluate the spatial autocorrelation function and, thereby, see how quickly various near-surface atmospheric variables lose correlation with increasing separation. The variables that the five ASFG SHEBA sites measured include near-surface barometric pressure, wind speed, direction, air temperature, and relative humidity; surface temperature; the four broadband radiation components, incoming and outgoing longwave and shortwave radiation; and the turbulent surface fluxes of momentum and sensible heat. For each site, we were also able to run the bulk flux algorithm that Andreas et al. (2010a, 2010b) developed to compute the surface fluxes of momentum and sensible and latent heat.

Not only will our analysis have implications for three-dimensional modeling with climate models and weather forecast models, it is germane to one-dimensional modeling—with PIEKTUK-D (Chung et al. 2011), for example, or with single-column models (e.g., Morrison et al. 2005). That is, our analysis should shed light on the area over which a one-dimensional model's results are valid. Likewise, our analysis will provide guidance on how far data measured on buoys drifting in sea ice can be extrapolated. Conversely, this correlation analysis can be used to decide how closely drifting buoys or other such observational platforms must be placed to provide data that cover specific regions or the entire Arctic.

Here, we divide the SHEBA data series into the four typical Arctic seasons (e.g., Lindsay 1998; Brunke et al. 2006)—fall (September, October, November), winter (December, January, February), spring (March, April, May), and summer (June, July, August)—and calculate spatial correlation functions in each season.

For brevity, we report on only a few of the available near-surface variables: namely, surface-level pressure, incoming longwave radiation, 2-meter air temperature, 2-meter relative humidity, and measured and bulk surface momentum fluxes (represented as friction velocities). A more encompassing analysis that will also include other metrics for assessing spatial variability will follow in a journal article.

We find that near-surface state variables like pressure, air temperature, and wind speed are well correlated in all seasons and for all separations up to the distance limit in our data, 12 km. Although relative humidity, on the other hand, generally shows weaker correlation, we ultimately decide that this result is probably an instrumentation problem.

Incoming longwave radiation shows mixed results. The spatial correlation is good in spring and summer, when the cloud cover was typically

* *Corresponding author address:* Dr. Edgar L Andreas, NorthWest Research Associates, Inc., 25 Eagle Ridge, Lebanon, NH 03766-1900; e-mail: eandreas@nwra.com.

100%, but is poorer for fall and winter, when fractional cloud cover was more common.

The friction velocity, u_*, measured by eddy covariance shows nearly constant correlation coefficients of roughly 0.8 for all separations. The bulk friction velocity, which depends strongly on the mean surface-level wind speed, likewise demonstrates no loss of correlation with increasing separation up to 12 km and has higher correlation coefficients—typically above 0.9. These two comparative analyses hint at the random variability inherent in turbulence measurements.

2. SHEBA DATA

The SHEBA Atmospheric Surface Flux Group (ASFG) dataset that we consider here comprises observations at five levels on the main 20-m tower (Persson et al. 2002; Grachev et al. 2005). Each tower level had a three-axis sonic anemometer/thermometer that yielded the mean wind speed and direction and the turbulent fluxes of momentum and sensible heat by eddy covariance. Each level also had instruments that measured mean air temperature and relative humidity. Here, we report the relative humidity with respect to ice saturation as opposed to water saturation, which is what the instruments actually reported (Andreas et al. 2002).

The lower four levels on the tower were, nominally, at 2.2, 3.2, 5.1, and 8.9 m; the upper level changed from 13.8 m in winter to 18.2 m in summer (Persson et al. 2002; Brunke et al. 2006). For the temperature, humidity, and wind speed measurements analyzed here, we used data from the lowest level that reported good data. This was generally the 2.2-m level. For the momentum and sensible heat fluxes, we used the median values from all levels that reported good data (Andreas et al. 2010a, 2010b).

Near this main tower were paired up-looking and down-looking broadband shortwave and longwave radiometers. These were equipped with blowers to mitigate frost formation on the radiometer domes. We calculated surface temperature with the data from the up-looking and down-looking longwave radiometers (Andreas et al. 2010a, 2010b).

The four remote sites, which were off the power grid for the main SHEBA camp, were instrumented with Flux-PAM stations (PAM means portable automated mesonet) from the instrument pool at the National Center for Atmospheric Research (Militzer et al. 1995; Horst et al. 1997). These were from 0.25 to 12 km from the main camp and measured the same variables that the main ASFG site did but at one level only (cf. Brunke et al. 2006; Andreas et al. 2010a, 2010b). That is, wind speed, direction, air temperature, relative humidity, momentum flux, and sensible heat flux were measured at single levels that were 2–3 m above the surface. We will henceforth refer to all of these low-level wind speed, temperature, and humidity data as the 2-m values.

Each PAM site also measured broadband incoming and outgoing longwave and shortwave radiation. Because of high relative humidity throughout the year (Andreas et al. 2002), early in the experiment, the domes of these radiometers were prone to frost formation that compromised their measurements. And such icing was not obvious in the radiometer data. In March and early April 1998, however, all PAM radiometers were fitted with heaters and blowers that kept the domes ice free through the end of the experiment.

Along with the main tower, three PAM sites ran for the entire SHEBA year: Atlanta, Baltimore, and Florida. Site Cleveland was also deployed early in the experiment but was damaged by a ridging event in early February 1998 and went off line for several months for repairs. This equipment was redeployed in mid-April 1998 at a site called Seattle and repositioned again in mid-June to a site called Maui. We will refer to the data stream from this PAM station as C-S-M (i.e., Cleveland-Seattle-Maui).

All data from the main camp instruments and these PAM sites were averaged hourly. In our subsequent correlation analysis, we use these simultaneous hourly data in our calculations.

Each of these five locations also had a GPS that reported hourly latitude (Θ) and longitude (Φ).

Figure 1 shows the connections among the sites. For our correlation calculations, we look at simultaneous values of the same variable from paired sites. Because we have five sites and are looking for pairs, we evaluate the number of combinations when five objects are considered two at a time; mathematically, this is

$$C(5,2) = \binom{5}{2} = \frac{5!}{2!(5-2)!} = 10\,. \qquad (1)$$

In other words, at each hour, we can have up to ten different distances to use in our computing the spatial correlation function for any of 15 variables.

Figure 2 shows a histogram of the hours of

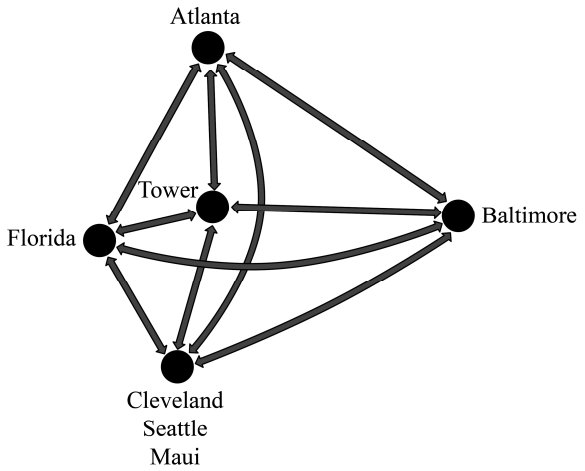

FIG. 1. When we pair the five SHEBA sites two at a time for the correlation analysis, we have ten potential separation distances for each hour.

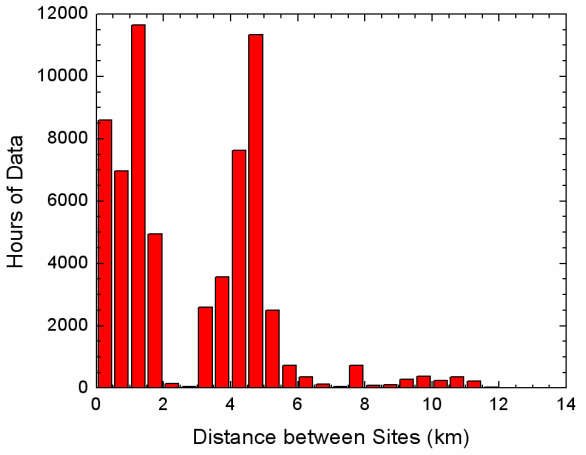

FIG. 2. This histogram shows the number of hours of unique site pairings that are available within the SHEBA dataset for each distance interval of 0.5 km.

unique data available for each distance. Each distance bin in the figure is 0.5 km wide.

If (Θ_A, Φ_A) represents the latitude and longitude at site A and if (Θ_B, Φ_B) represents the latitude and longitude at site B, we calculated the distance D between the two sites as (e.g., Weaver and Mirouze 2013)

$$D = R\Delta\Omega . \tag{2}$$

Here, R (= 6372.8 km) is the radius of curvature of the Earth and

$$\Delta\Omega = 2\arcsin\left\{\left[\sin^2\left(\frac{\Delta\Theta}{2}\right) + \cos\Theta_A \cos\Theta_B \sin^2\left(\frac{\Delta\Phi}{2}\right)\right]^{1/2}\right\} \tag{3}$$

is the arc length, where $\Delta\Theta = \Theta_A - \Theta_B$ and $\Delta\Phi = \Phi_A - \Phi_B$.

From Fig. 2, we see that the vast majority of separations in our dataset are 6 km and less. Most of the separations beyond 6 km occurred in September 1998, when Baltimore drifted rapidly away from the other sites. That is, the largest separations arise from September data when Baltimore is paired with the other four sites.

3. CORRELATION CALCULATIONS

To compute the spatial correlation function for variable V in each season, we start by computing the covariance (Cov) for variable V between sites A and B when they have separation D, where D represents the averaging interval [D_-, D_+) and $D_+ - D_- = 0.5\,\text{km}$. That is, we compute this covariance as

$$\mathrm{Cov}_{V,AB}(D) = \frac{1}{N_D}\sum_{i=1}^{N_D}\left[V_{Ai}(P_A) - \overline{V}_{AD}\right] \bullet \left[V_{Bi}(P_B) - \overline{V}_{BD}\right] . \tag{4}$$

Here, P_A, for example, is the position of site A, represented as (Θ_A, Φ_B), and N_D is the number of good A and B pairs for variable V that are in distance interval [D_-, D_+) for a given season. Subscript i is the index for a specific hour in the dataset. Furthermore,

$$\overline{V}_{XD} = \frac{1}{N_D}\sum_{i=1}^{N_D} V_{Xi}(D) \tag{5}$$

is the average of these same data, where X denotes site A or B.

To calculate the spatial correlation function, we also need the standard deviations (σ_V) for sites A and B for variable V for the given season when the separation is in the distance interval [D_-, D_+). These come from the variances as

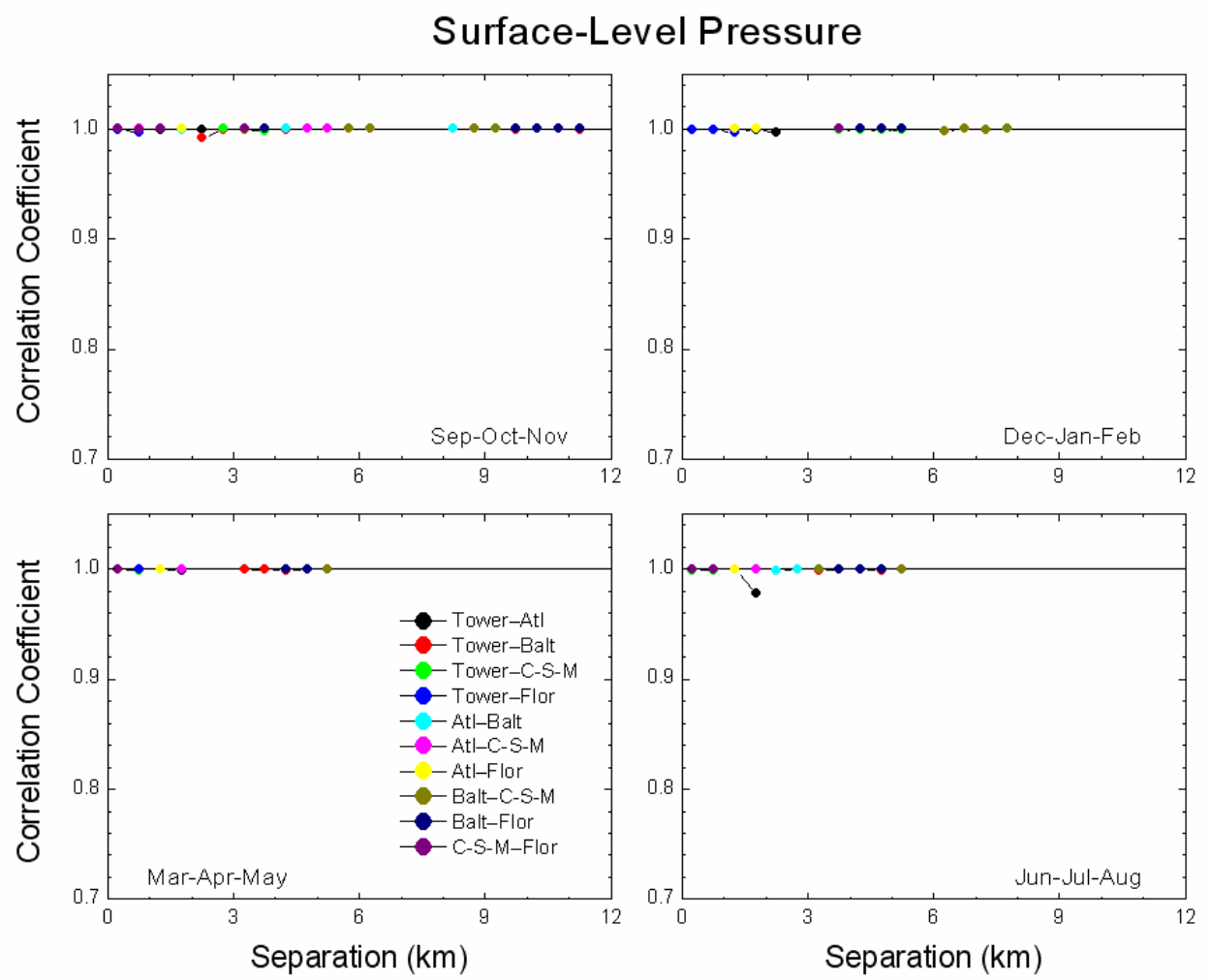

FIG. 3. Spatial correlation functions for surface-level pressure in each of four seasons: fall (SON), winter (DJF), spring (MAM), and summer (JJA). The legend shows the data pairs used in the correlation calculations, (7).

$$\sigma^2_{V,X}(D) = \frac{1}{N_D}\sum_{i=1}^{N_D}\left(V_{Xi} - \overline{V}_{XD}\right)^2, \qquad (6)$$

where subscript X again denotes either site A or B.

From (4), (5), and (6), we ultimately compute the spatial correlation function for variable V, separation D, a given season, and sites A and B as

$$\rho_{V,AB}(D) = \frac{Cov_{V,AB}(D)}{\sigma_{V,A}(D)\sigma_{V,B}(D)}. \qquad (7)$$

This $\rho_{V,AB}$ has the same properties as usual correlation coefficients. It ranges from –1.00 to +1.00. If $N_D = 1$, it is undefined because both variances are zero. If $N_D = 2$, $\rho_{V,AB}$ is exactly +1.00 or –1.00: Two points define a straight line, which has perfect positive or negative correlation.

We used the algorithm in Bendat and Piersol (1971, p. 126ff.) to evaluate 95% confidence intervals for our calculated $\rho_{V,AB}(D)$ values. These estimates suggest that we cannot have much confidence in correlation values that are based on pairings for which $N_D < 15$. In the following plots, we therefore eliminated any $\rho_{V,AB}(D)$ values that resulted from fewer than 15 paired observations.

4. RESULTS

As an example of very good—almost perfect—correlation, we display in Fig. 3 the

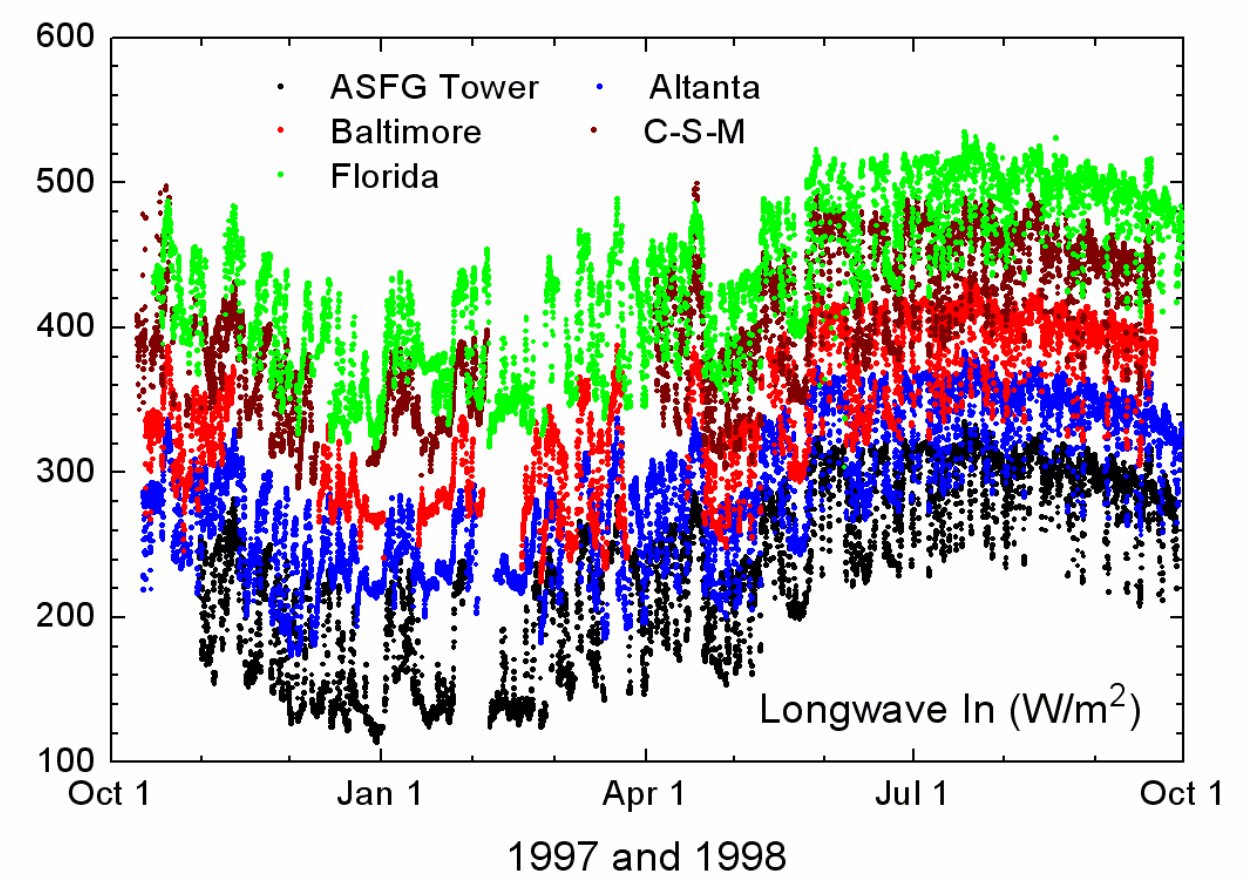

FIG. 4. Hourly observations for the entire year of incoming longwave radiation at each site maintained by the SHEBA Atmospheric Surface Flux Group: the main tower and Flux-PAM sites Atlanta, Baltimore, C-S-M, and Florida. The ASFG Tower series is the baseline; Atlanta, Baltimore, C-S-M, and Florida are sequentially offset by 50 W m^{-2} for easier viewing.

spatial correlation functions for pressure for the four seasons. Here, the correlation is virtually 1.00 for all separations and all seasons; it shows no tendency to decrease with increasing separation. Clearly, Arctic pressure gradients are weak.

Figure 4 shows time series of all the hourly ASFG observations of incoming longwave radiation, $Q_{L\downarrow}$, for the entire SHEBA year. The ASFG Tower series has a big gap around February 1, when a lead cut the ice camp in two and disrupted power to the ASFG instruments in the main camp. The series from Flux-PAM sites C-S-M is especially spotty for the first six months; the longest gap is from early February until early April, when the instruments were being repaired after the ridging event damaged them.

Figure 5 shows the spatial correlation functions computed from these series of incoming longwave radiation. In fall and winter, the correlation tends to be erratic. Correlations, nevertheless, are generally above 0.8.

The correlations for large separation in the September-October-November panel are especially noteworthy because all of these came from pairings involving Baltimore in September 1998, long after we had remedied the problem of radiometer icing. Therefore, the correlation values of about 0.90–0.95 should be representative of fall. At other times in fall and winter, the correlations may be erratic because of missing data (i.e., small numbers of samples) or because we were unable to identify data that were affected by the icing and, thus, inadvertently retained them in our analyses.

By early April 1998, however, we had remedied the problem of radiometer icing

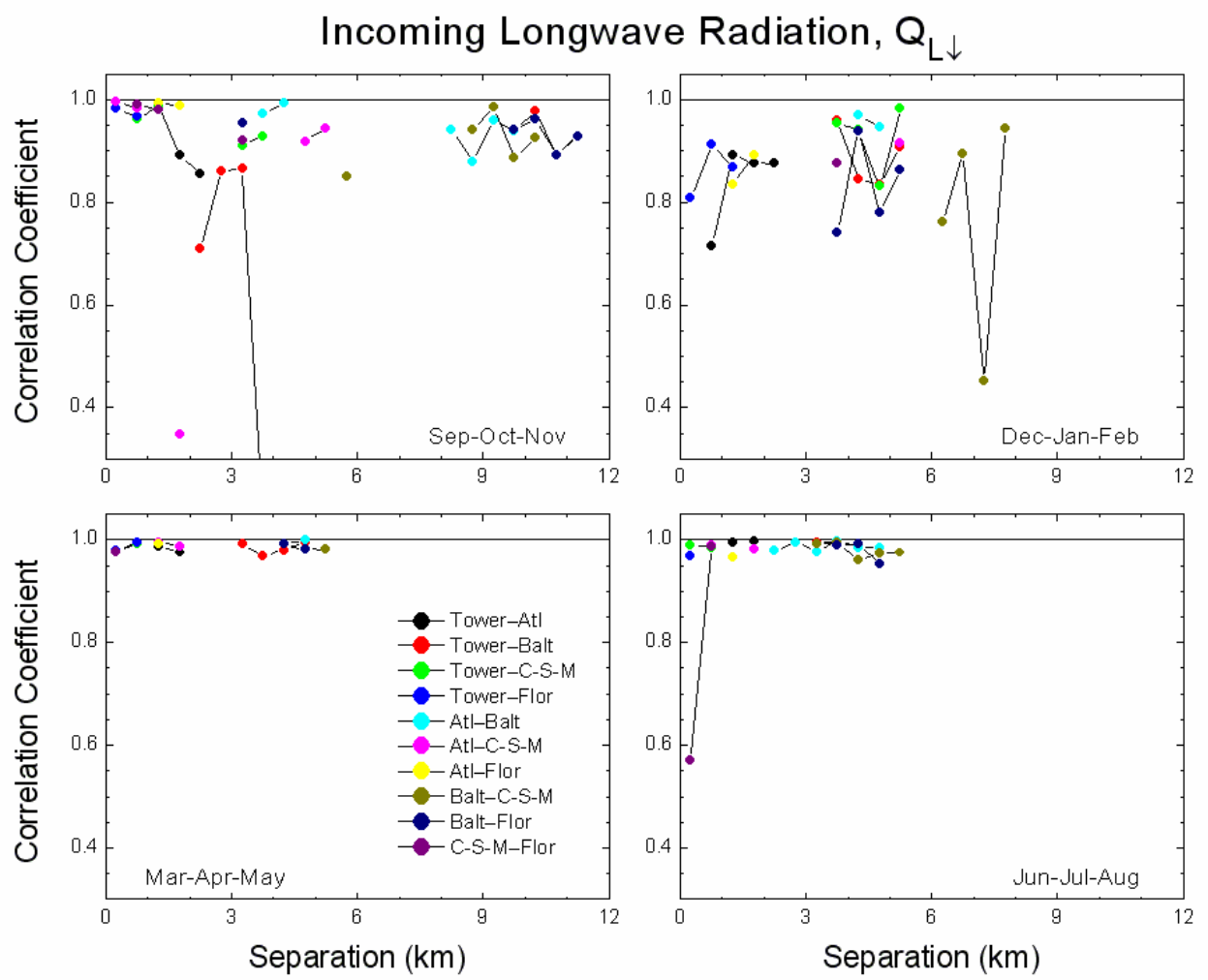

FIG 5. As in Fig. 3, but this figure shows the spatial correlation functions for incoming longwave radiation.

(Andreas et al. 2010a, 2010b); therefore, we have more confidence in the correlation functions for spring and summer, almost all of which have values above 0.95. Moreover, again none of the panels in Fig. 5 show any tendency for the correlation to decrease with increasing separation.

Figure 6 may explain the correlations we see in Fig. 5. It shows hourly estimates of the cloud fraction observed in the main SHEBA camp by the remote sensing instruments operated by NOAA's Earth System Research Laboratory (Intrieri et al. 2002; Shupe et al. 2006). These data come from Matt Shupe, Janet Intrieri, and Taneil Uttal (2010, personal communication). Polar cloud fraction tends to be bimodal: It is typically either 0 or 100% (e.g., Makshtas et al. 1999). But that behavior varies seasonally. In Fig. 6, we see the predominance of total cloud cover in the spring and summer. That is, cloud fraction is mostly 100% in these seasons. In the fall and winter, on the other hand, periods with no clouds occur more frequently; and partial cloud clover is more frequent than in spring and summer.

We speculate that the partial cloud cover in fall and winter, at least in part, explains why the correlations in these seasons in Fig. 5 are lower than in spring and summer. Radiometers at different sites may have been seeing different sky conditions. In contrast, the generally full cloud cover of spring and summer would have made the radiative environment more uniform than in fall and winter.

Figure 7 is the time series of 2-m air temperature from each of the five SHEBA sites. Temperatures start well below freezing in October 1997, fall to near –40°C in December and

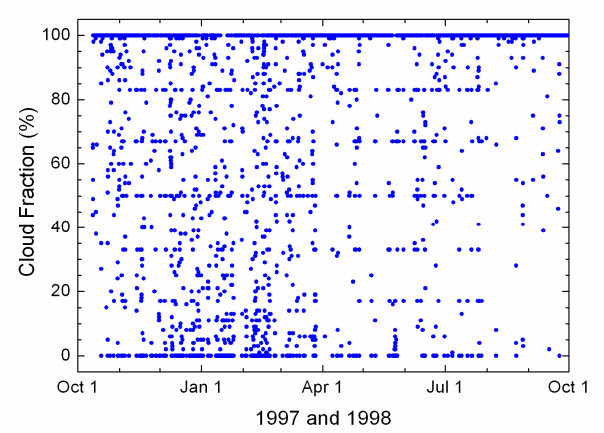

FIG. 6. Hourly cloud fraction for the SHEBA year as determined by the NOAA remote sensing instruments operating in the main camp. The data are courtesy of Matt Shupe, Janet Intrieri, and Taniel Uttal (2010, personal communication).

January, then rise slowly, and hover around 0°C for the three months of summer. As with the radiation series in Fig. 4, we see breaks in the series during the first six months, especially in the Cleveland-Seattle-Maui series.

Despite these breaks, the spatial correlation functions for temperature (Fig. 8) are generally above 0.95 in all seasons. And once more, we see no tendency for the correlation functions to fall off with increasing spatial separation. The surface-level air temperature, thus, appears to change uniformly over sea ice in all seasons—at least over distances less than 12 km.

Similarly, we find that the wind speed at 2 m is well correlated in all seasons (not shown). Correlation values tend to be slightly lower than for air temperature—they are typically above 0.9—but likewise have no tendency to decrease with spatial separation. Hence, for this state variable, too, we

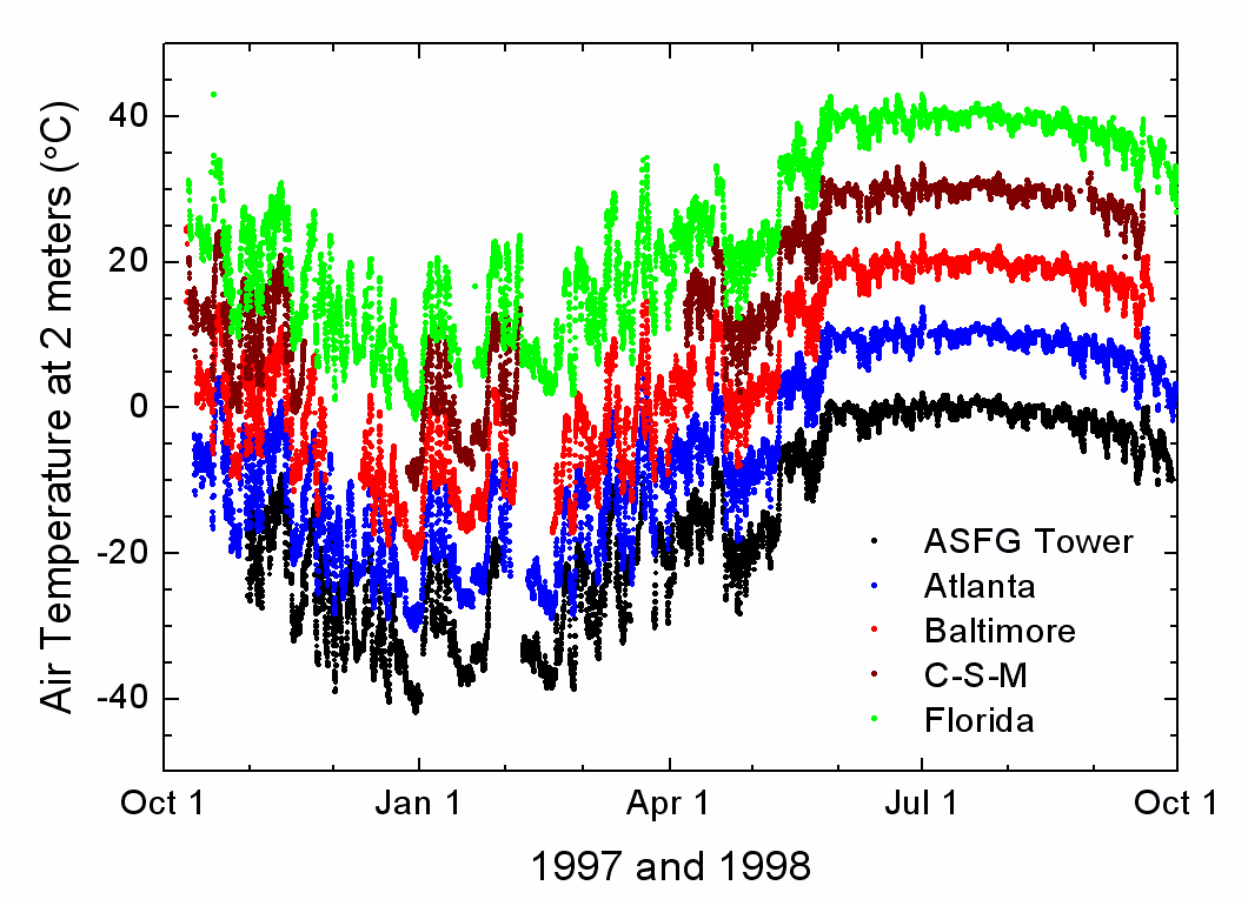

FIG. 7. As in Fig. 4, but this shows hourly time series of 2-meter air temperature at each of the five sites for the entire SHEBA year. Again, the ASFG Tower series is the baseline; the remaining four sites are sequentially offset by 10°C to facilitate viewing.

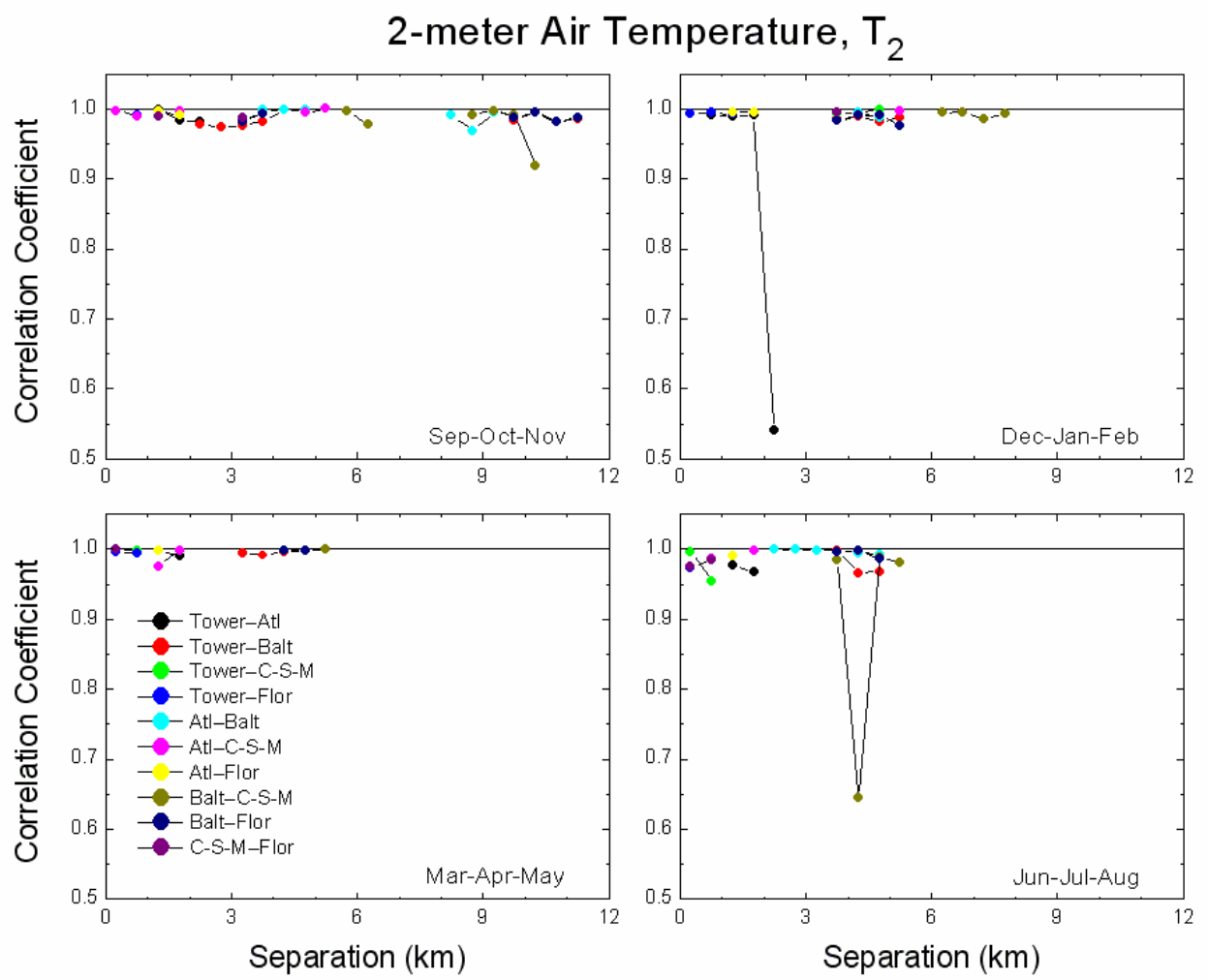

FIG. 8. As in Fig. 3, but this figure shows the spatial correlation functions for 2-m air temperature.

confirm coherence in changes in wind speed over distances up to 12 km.

Relative humidity, however, is a state variable with disconcerting behavior. Figure 9 shows hourly time series of relative humidity from each site for the entire SHEBA year; Fig. 10 gives the spatial correlation functions for each season.

Andreas et al. (2002) demonstrated that relative humidity measured over sea ice should be calculated with respect to saturation over ice in all seasons because it then is always near 100%. Figure 9 reiterates this result. Although the relative humidity series are variable, especially in spring and summer, values hover around 100%.

Despite this consistent behavior among the five SHEBA sites, the spatial correlation functions in Fig. 10 are not consistent. In particular, pairs for which one of the sites is the ASFG tower generally have poor correlation.

The analysis in Andreas et al. (2002) helps explain this behavior, as does scrutinizing Fig. 9. The relative humidity measurements at SHEBA were made with Vaisala capacitance sensors. The five sensors on the ASFG tower were model HMP235; the Flux-PAM stations all used model HMD50Y sensors. Figures 7, 8, and 11 in Andreas et al. demonstrate that these two sensor types had different response characteristics, especially at air temperatures below –20°C.

Figure 9 also suggests diverse behavior. In early January, for instance, the trace from the ASFG tower has a down-going excursion that lasts over a week. At the same time, though, the traces from the four PAM sites have up-going excursions. And we see other instances of such contrasting responses in the traces in Fig. 9.

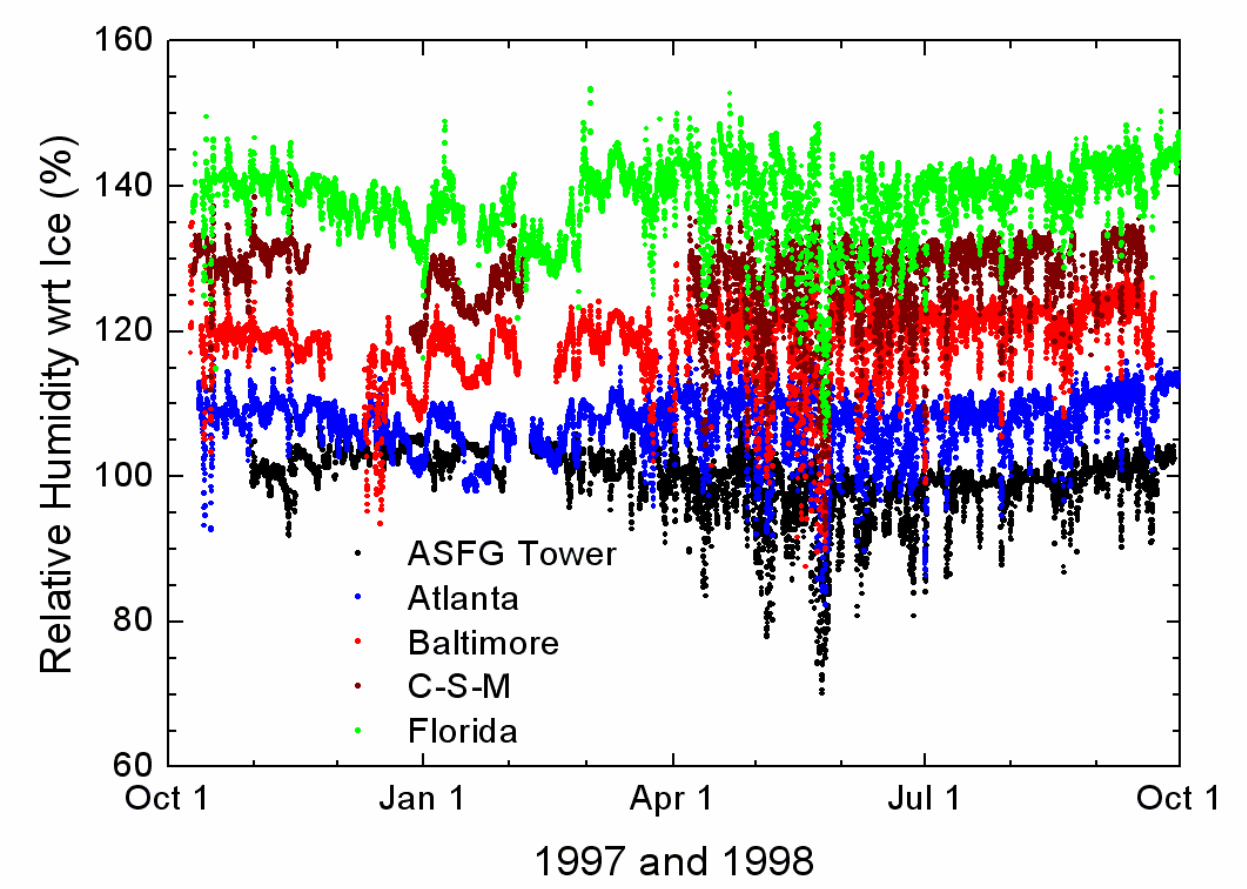

FIG. 9. As in Fig. 4, but these are the time series of 2-meter relative humidity with respect to saturation over ice. The ASFG Tower series is again the baseline; the four Flux-PAM series are sequentially offset from this series by 10%.

These instrumental differences between the ASFG tower sensors and the Flux-PAM sensors explain some of the poor correlation in Fig. 10. Notice, the lowest correlations usually involve the ASFG tower measurement paired with a PAM site. When two PAM sites are paired, the correlations are typically above 0.8. In other words, for sensors having similar calibrations and response characteristics, relative humidity has high correlation that, again, does not obviously degrade with sensor separation.

The turbulent fluxes that the SHEBA Atmospheric Surface Flux Group measured were the surface fluxes of momentum (τ) and sensible (H_s) and latent (H_L) heat. We report here only on the momentum flux; but because we discuss both the measured flux and the comparable flux from a bulk flux algorithm, we need to briefly describe that algorithm.

The turbulent fluxes and their parameterizations generally take the form (e.g., Fairall et al. 1996, 2003; Andreas et al. 2010a, 2010b)

$$\tau = -\rho\overline{uw} = \rho u_*^2 = \rho C_{Dr} S_r^2 , \qquad (8a)$$

$$H_s = \rho c_p \overline{w\theta} = \rho c_p C_{Hr} S_r (\Theta_s - \Theta_r) , \qquad (8b)$$

$$H_L = \rho L_v \overline{wq} = \rho L_v C_{Er} S_r (Q_s - Q_r) . \qquad (8c)$$

Here, u, w, θ, and q are, respectively, the turbulent fluctuations in the along-wind velocity, vertical velocity, air temperature, and specific humidity. The overbars denote time averages. S_r, Θ_r, and Q_r are average effective wind speed, potential temperature, and specific humidity at reference height r; Θ_s and Q_s are the average potential temperature and specific humidity at the surface.

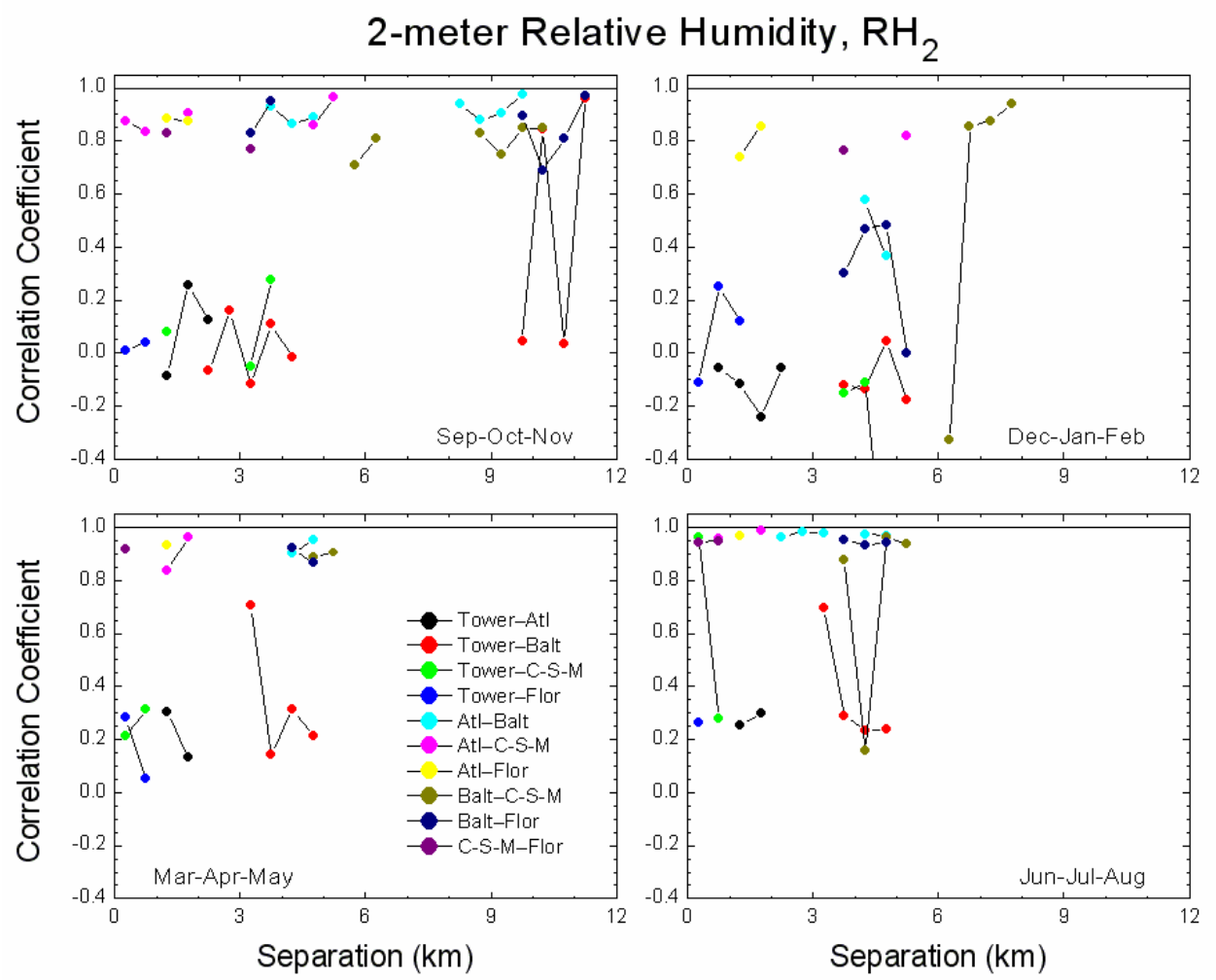

FIG. 10. As with Fig. 3, but this figure shows the spatial correlation functions for the relative humidity at 2 m with respect to saturation over ice.

We always evaluate Q_s as the saturation value at Θ_s. The ρ, c_p, and L_v are the air density, the specific heat of air at constant pressure, and the latent heat of vaporization or sublimation. Equation (8a) also defines the friction velocity, u_*.

From measurements of $\overline{uw}$, $\overline{w\theta}$, $\overline{wq}$, S_r, Θ_r, Q_r, and Θ_s, Andreas et al. (2010a, 2010b) developed parameterizations for the turbulent transfer coefficients C_{Dr} (the drag coefficient appropriate for height r), C_{Hr}, and C_{Er} (the scalar transfer coefficients for height r).

In a model or a standalone analysis, the right sides of (8) are solved iteratively to compute the fluxes. Other equations in this iteration are the parameterizations for C_{Dr}, C_{Hr}, and C_{Er} and an equation for the Obukhov length, L, on which the transfer coefficients depend. This is

$$L = -\left[\frac{kg}{\overline{T}u_*^3}\left(\frac{H_s}{\rho c_p} + \frac{0.61\overline{T}}{1+0.61\overline{Q}}\frac{H_L}{\rho L_v}\right)\right]^{-1}. \quad (9)$$

Here, g is the acceleration of gravity; k (= 0.40), the von Kármán constant; and $\overline{T}$ and $\overline{Q}$, average air temperature and specific humidity in the near-surface layer.

In the discussion to follow, we use u_* to represent the momentum flux. Figure 11 shows the spatial correlation functions for the SHEBA measurements of u_*. Figure 12 is a comparable plot for the u_* values derived from the Andreas et al. (2010a, 2010b) bulk flux algorithm.

Figures 11 and 12 have contrasting behaviors. Correlations are typically above 0.9 in

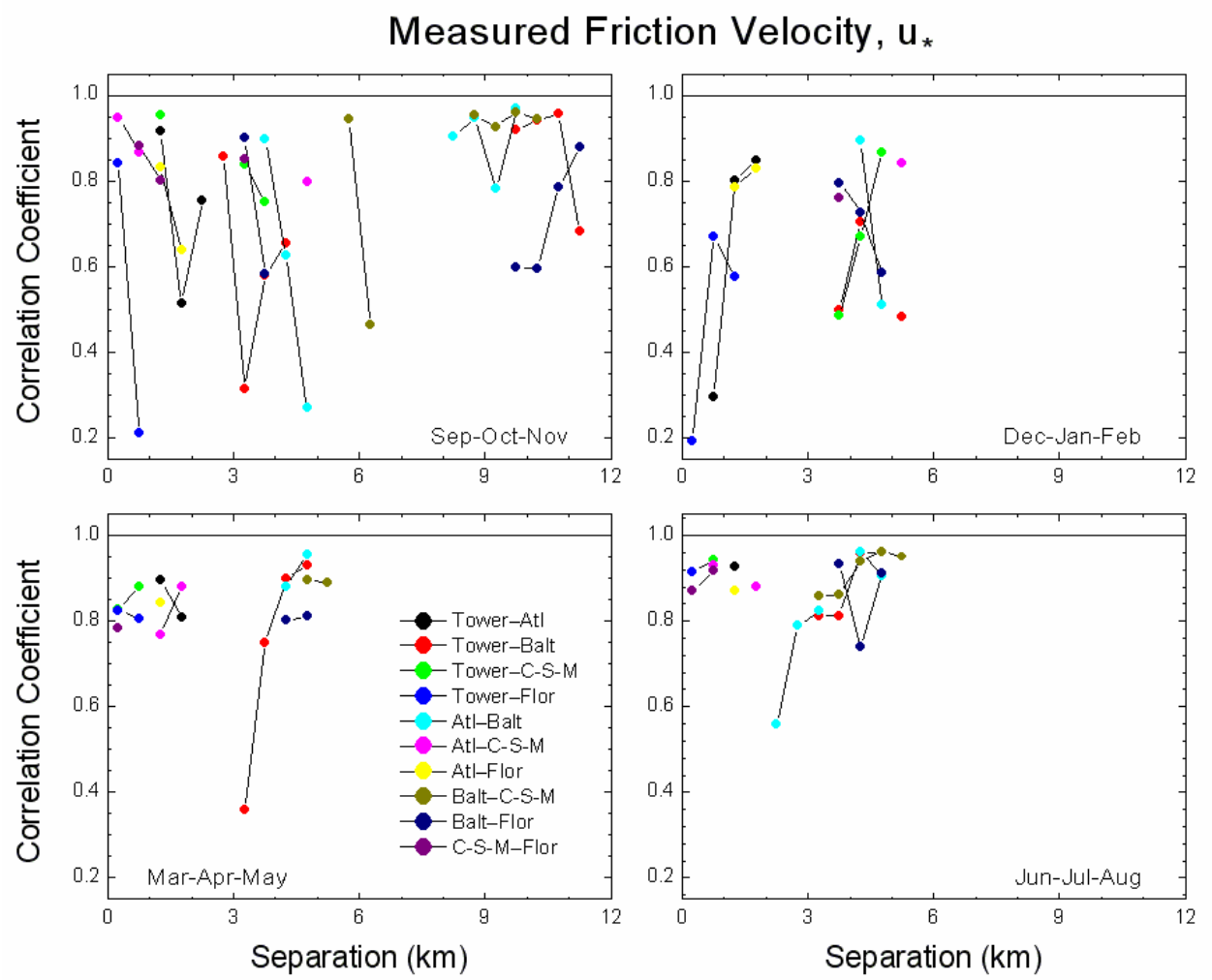

FIG. 11. As with Fig. 3, but these are the spatial correlation functions for the measured friction velocity, u_*, which we use to represent the momentum flux, τ.

Fig. 12, which is for bulk u_*. For the u_* measurements, however, Fig. 11, the correlation functions are more erratic, especially in fall and winter. We attribute some of this erratic behavior in fall and winter to instrument problems. The sonic anemometers on the PAM stations were prone to icing that ruined the measurements and led to missing data up to early March 1998, when we added heating to keep the sensors ice free. The correlations functions for large separations in fall (the September, October, November panel) support this appraisal. These calculations all came from pairings with Baltimore for September 1998, when the sonic anemometers were heated and no longer suffered icing. During this period, the correlation coefficients are less erratic and often are above 0.8, as they are for spring and summer, which were also after heating for the sonics eliminated any icing.

Nevertheless, the correlation functions for the bulk u_* are generally better in all seasons than this 0.8 level; typically, the correlation functions for bulk u_* are above 0.9. First, all turbulence measurements are subject to random errors. Such errors limit how good the correlations can be in Fig. 11. Second, the bulk estimates of u_* derive, primarily, from the measurements of average wind speed and also depend on average air temperature and humidity through the iterations necessary in the bulk flux algorithm; see (8). But we have seen that average wind speed and temperature have good spatial correlation. The correlation functions for bulk u_*, thus, should also.

In summary, while we cannot unequivocally

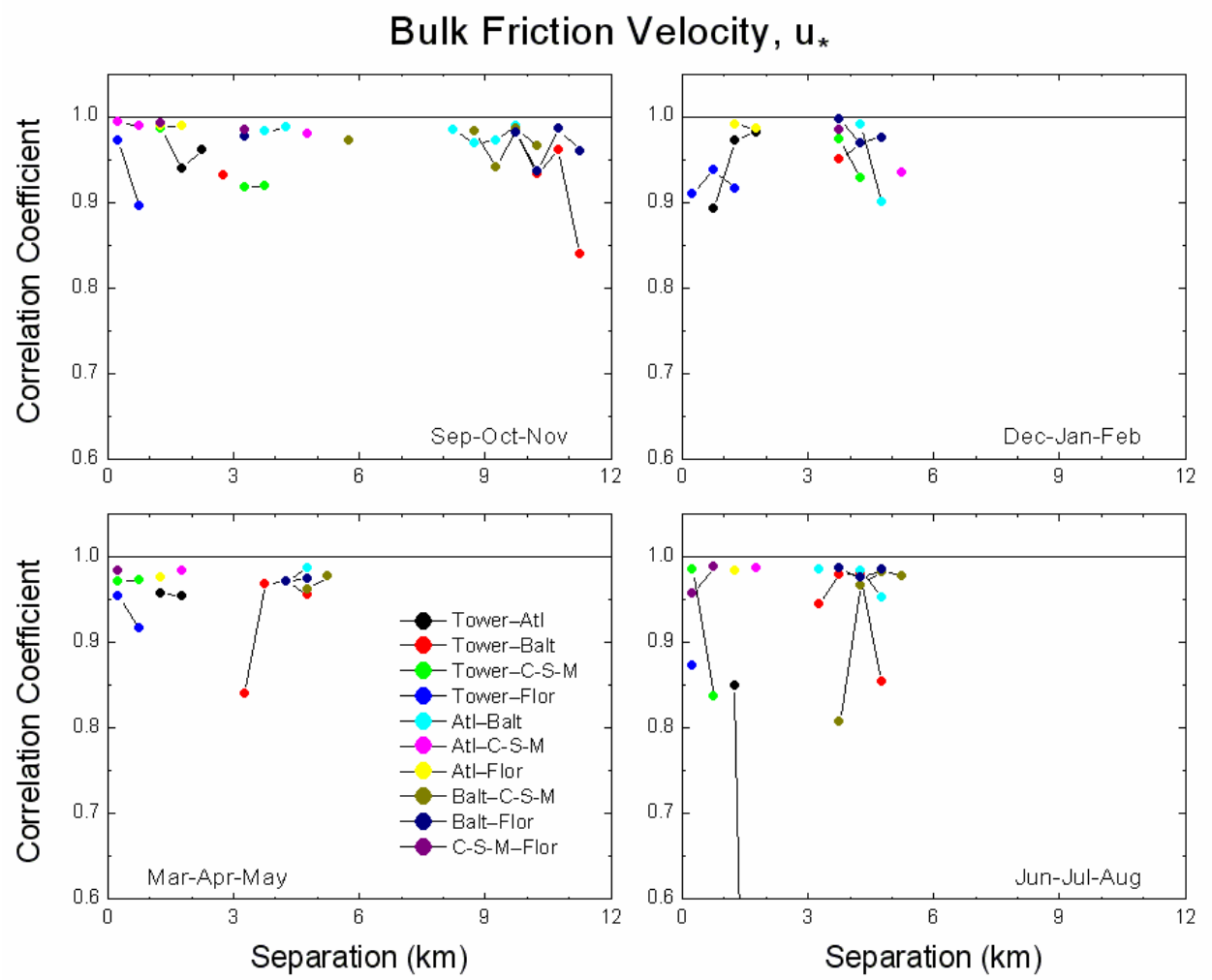

FIG. 12. As in Fig. 11, but these are the spatial correlation functions for the friction velocity computed from the Andreas et al. (2010a, 2010b) bulk flux algorithm.

say that the measured momentum flux is coherent over grid cells with dimensions up to 12 km, the data do hint at this conclusion. The momentum flux that a model might yield, however, should be coherent over a grid cell, as evidenced by Fig. 12.

5. CONCLUSIONS

We had hypothesized that spatial correlation functions for surface-level variables over Arctic sea ice would decay with increasing separation between measurement sites. We saw no evidence, however, of such loss of correlation with increasing separation for any of the variables that we presented here—at least for separations up to 12 km. Most of the correlation coefficients that we calculated were not perfect, but they were independent of spatial separation.

State variables like pressure, wind speed, and air temperature had high correlation—typically above 0.9—and pressure had near-perfect correlation. As a result, the assumption that such variables behave coherently over computer grid cells of at least 12 km is appropriate. Another state variable, relative humidity, behaved more erratically; but we presume that its poorer correlation resulted from instrument problems since Andreas et al. (2002) had earlier demonstrated that the relative humidity at all SHEBA sites in all seasons was very near 100% when figured with respect to saturation over ice.

We looked here at only one of the available turbulence variables—friction velocity, u_*. For periods when all five SHEBA sites had sonic

anemometers that were unaffected by icing, the spatial correlation function was typically 0.8 or above. At times when icing was affecting the sonic measurements, correlations were erratic and much lower. For the friction velocities computed with the Andreas et al. (2010a, 2010b) bulk flux algorithm, the spatial correlation functions were typically above 0.9 in all seasons.

These two comparative analyses hint at the inherent random variability in turbulence measurements that explains the relatively lower correlations for the measured u_*. The bulk u_*, on the other hand, derived from state variables, which we demonstrated had very good spatial correlation. Because computer models can predict only the bulk u_*, assuming that this variable behaves coherently over a grid cell containing sea ice is justified.

6. ACKNOWLEDGMENTS

We thank our colleagues in the SHEBA Atmospheric Surface Flux Group, who helped us collect, process, and interpret the SHEBA data: Chris Fairall, Andrey Grachev, Peter Guest, Tom Horst, and Ola Persson. We also thank Matt Shupe, Janet Intrieri, and Taneil Uttal for the synthesized cloud fraction data that went into Fig. 6. Lastly, we thank Emily Moynihan of BlytheVisual for creating Fig. 1 and the U.S. National Science Foundation, which supported this work with award ARC 10-19322.

7. REFERENCES

Andreas, E. L, C. W. Fairall, P. S. Guest, and P. O. G. Persson, 1999: An overview of the SHEBA atmospheric surface flux program. Preprints, *Fifth Conf. on Polar Meteorology and Oceanography*, Dallas, TX, Amer. Meteor. Soc., 411–416.

____, P. S. Guest, P. O. G. Persson, C. W. Fairall, T. W. Horst, R. E. Moritz, and S. R. Semmer, 2002: Near-surface water vapor over polar sea ice is always near ice saturation. *J. Geophys. Res.*, **107** (C10, 8033), doi: 10.1029/2000JC000411.

____, T. W. Horst, A. A. Grachev, P. O. G. Persson, C. W. Fairall, P. S. Guest, and R. E. Jordan, 2010a: Parameterising turbulent exchange over summer sea ice and the marginal ice zone. *Quart. J. Roy. Meteor. Soc.*, **136**, 927–943.

____, P. O. G. Persson, R. E. Jordan, T. W. Horst, P. S. Guest, A. A. Grachev, and C. W. Fairall, 2010b: Parameterizing turbulent exchange over sea ice in winter. *J. Hydrometeor.*, **11**, 87–104.

Bendat, J. S., and A. G. Piersol, 1971: *Random Data: Analysis and Measurement Procedures*. Wiley-Interscience, 407 pp.

Bromwich, D. H., K. M. Hines, and L.-S. Bai, 2009: Development and testing of Polar Weather Research and Forecasting model: 2. Arctic Ocean. *J. Geophys. Res.*, **114** (D08122), doi:10.1029/2008JD010300.

Brunke, M. A., M. Zhou, X. Zeng, and E. L Andreas, 2006: An intercomparison of bulk aerodynamic algorithms used over sea ice with data from the SHEBA experiment. *J. Geophys. Res.*, **111** (C09001), doi: 10.1029/2005JC002907.

Chung, Y.-C., S. Bélair, and J. Mailhot, 2011: Blowing snow on Arctic sea ice: Results from an improved sea ice-snow-blowing snow coupled system. *J. Hydrometeor.*, **12**, 678–689.

Collins, W. D., and 14 others, 2006: The Community Climate System Model Version 3 (CCSM3). *J. Climate*, **19**, 2122–2143.

Fairall, C. W., E. F. Bradley, D. P. Rogers, J. B. Edson, and G. S. Young, 1996: Bulk parameterization of air-sea fluxes for Tropical Ocean-Global Atmosphere Coupled-Ocean Atmosphere Response Experiment. *J. Geophys. Res.*, **101** (C2), 3747–3764.

____, ____, J. E. Hare, A. A. Grachev, and J. B. Edson, 2003: Bulk parameterization of air-sea fluxes: Updates and verification for the COARE algorithm. *J. Climate*, **16**, 571–591.

Grachev, A. A., C. W. Fairall, P. O. G. Persson, E. L Andreas, and P. S. Guest, 2005: Stable boundary-layer scaling regimes: The SHEBA data. *Bound.-Layer Meteor.*, **116**, 201–235.

Horst, T. W., S. P. Oncley, and S. R. Semmer, 1997: Measurement of water vapor fluxes using capacitance RH sensors and cospectral similarity. Preprints, *12th Symp. on Boundary Layers and Turbulence*, Vancouver, B.C., Amer. Meteor. Soc., 360–361.

Hunke, E. C., W. H. Lipscomb, and A. K. Turner, 2010: Sea-ice models for climate study: Retrospective and new directions. *J. Glaciol.*, **56**, 1162–1172.

Intrieri, J. M., C. W. Fairall, M. D. Shupe, P. O. G. Persson, E. L Andreas, P. S. Guest, and R. E. Moritz, 2002: An annual cycle of Arctic surface cloud forcing at SHEBA. *J. Geophys.*

Res., **107** (C10, 8039), doi: 10.1029/2000JC000439.

Lindsay, R. W., 1998: Temporal variability of the energy balance of thick Arctic pack ice. *J. Climate*, **11**, 313–333.

Makshtas, A. P., E. L Andreas, P. N. Svyaschennikov, and V. F. Timachev, 1999: Accounting for clouds in sea ice models. *Atmos. Res.*, **52**, 77–113.

Militzer, J. M., M. C. Michaelis, S. R. Semmer, K. S. Norris, T. W. Horst, S. P. Oncley, A. C. Delany, and F. V. Brock, 1995: Development of the prototype PAM III/Flux-PAM surface meteorological station. Preprints, *Ninth Symp. on Meteorological Observations and Instrumentation*, Charlotte, NC, Amer. Meteor. Soc., 490–494.

Morrison, H., J. A. Curry, M. D. Shupe, and P. Zuidema, 2005: A new double-moment microphysics parameterization for application in cloud and climate models: Part II. Single-column modeling of Arctic clouds. *J. Atmos. Sci.*, **62**, 1678–1693.

Persson, P. O. G., C. W. Fairall, E. L Andreas, P. S. Guest, and D. K. Perovich, 2002: Measurements near the Atmospheric Surface Flux Group tower at SHEBA: Near-surface conditions and surface energy budget. *J. Geophys. Res.*, **107** (C10, 8045), doi: 10.1029/2000JC000705.

Shupe, M. D., S. Y. Matrosov, and T. Uttal, 2006: Arctic mixed-phase cloud properties derived from surface-based sensors at SHEBA. *J. Atmos. Sci.*, **63**, 697–711.

Tastula, E.-M., T. Vihma, and E. L Andreas, 2012: Evaluation of Polar WRF from modeling of the atmospheric boundary layer over Antarctic sea ice in autumn and winter. *Mon. Wea. Rev.*, **140**, 3919–3935.

Uttal, T., and 27 others, 2002: Surface Heat Budget of the Arctic Ocean. *Bull. Amer. Meteor. Soc.*, **83**, 255–275.

Weaver, A. T., and I. Mirouze, 2013: On the diffusion equation and its application to isotropic and anisotropic correlation modelling in variational assimilation. *Quart. J. Roy. Meteor. Soc.*, **139**, 242–260.